pISSN 2384-1095
eISSN 2384-1109

iMRI 2018;22:26-36

https://doi.org/10.13104/imri.2018.22.1.26

iMRI
Investigative Magnetic Resonance Imaging

Quantitative Evaluation of the First Order Creatine-Kinase Reaction Rate Constant in *in vivo* Shunted Ovine Heart Treated with Oxandrolone Using Magnetization Transfer ^{31}P Magnetic Resonance Spectroscopy (MT-^{31}P-MRS) and ^{1}H/^{31}P Double-Tuned Surface Coil: a Preliminary Study

Bijaya Thapa[1,2], Marjanna Dahl[3], Eugene Kholmovski[1,4], Phillip Burch[5], Deborah Frank[3], Eun-Kee Jeong[1,4]

[1]Utah Center for Advanced Imaging Research, University of Utah, Utah, USA
[2]Department of Physics and Astronomy, University of Utah, Utah, USA
[3]Department of Pediatrics, University of Utah, Utah, USA
[4]Department of Radiology and Imaging Sciences, University of Utah, Utah, USA
[5]Department of Surgery, University of Utah, Utah, USA

Original Article

Received: May 11, 2017
Revised: October 28, 2017
Accepted: December 27, 2017

Correspondence to:
Eun-Kee Jeong, Ph.D.
University of Utah, Utah Center for Advanced Imaging Research, Department of Radiology,
729 Arapeen Drive, Salt Lake City, Utah 84108, USA
Tel. +1-801-581-8643
Fax. +1-801-585-2592
E-mail: ekj@ucair.med.utah.edu

Purpose: Children born with single ventricle physiology demonstrate poor growth rate and suffer from malnutrition, which lead to increased morbidity and mortality in this population. We assume that an anabolic steroid, oxandrolone, will promote growth in these infants by improving myocardial energy utilization. The purpose of this paper is to study the efficacy of oxandrolone on myocardial energy consumption in these infants.

Materials and Methods: We modeled single ventricle physiology in a lamb by prenatally shunting the aorta to the pulmonary artery and then postnatally, we monitored cardiac energy utilization by quantitatively measuring the first order reaction rate constant, k_f of the creatine-kinase reaction in the heart using magnetization transfer ^{31}P magnetic resonance spectroscopy, home built ^{1}H/^{31}P transmit/receive double tuned coil, and transmit/receive switch. We also performed cine MRI to study the structure and dynamic function of the myocardium and the left ventricular chamber. The spectroscopy data were processed using home-developed python software, while cine data were analyzed using Argus software.

Results: We quantitatively measured both the first order reaction rate constant and ejection fraction in the control, shunted, and the oxandrolone-treated lambs. Both k_f and ejection fraction were found to be more significantly reduced in the shunted lambs compared to the control lambs, and they are increased in oxandrolone-treated lambs.

Conclusion: Some improvement was observed in both the first order reaction rate constant and ejection fraction for the lamb treated with oxandrolone in our preliminary study.

Keywords: Single ventricle (SV) physiology; T/R switch; High-power radiofrequency (RF) switch; First order reaction rate (k_f); Ejection fraction (EF); Magnetic resonance imaging (MRI); Magnetic resonance spectroscopy (MRS)

INTRODUCTION

Infants with single ventricle (SV) physiology account for a significant proportion of child healthcare resources, but tools for efficient comparison of new or even standard treatment strategies are lacking. Multiple specific types of congenital cardiac malformations result in single ventricle physiology, including hypoplastic left heart syndrome and tricuspid atresia. The vast majority of SV infants require a series of two to three palliative surgeries (Fontan) (1) because the heart cannot be surgically corrected in ways to allow for normal cardiac physiology. SV infants have a mortality rate of approximately 25% in the first year of life and survivors experience a significant lifetime morbidity rate. Children, even those with excellent technical repairs, may slowly deteriorate in the postoperative period from multiple etiologies including wound infections, prolonged effusions, prolonged mechanical ventilation and venous thrombosis. Growth failure and malnutrition are complications common to virtually all of these populations (2), and poor growth is associated with increased morbidity and mortality (3). The growth failure factor found in SV infants may be due to the high cardiac energy requirements from their shunt dependent physiology (4, 5). The growth rate has been difficult to modify, and simply increasing the caloric intake or changing the method of feeding has not proven uniformly successful (6). We hypothesize that an anabolic steroid, oxandrolone will promote growth in SV infants by improving myocardial energy utilization.

Oxandrolone is approved to promote growth in children with histories of extensive surgery, severe trauma or burns, chronic infections, constitutional growth delay and those afflicted with Turner's syndrome (7–10). The most extensive clinical experience with the therapeutic use of oxandrolone may be seen in pediatric burn patients (11–13), in whom oxandrolone has been safely administered for one year, with beneficial effects on lean body mass and bone mineral content identifiable five years post-treatment (8). Echocardiographic evaluation in this study suggests more efficient myocardial energy usage in patients on oxandrolone, compared to the placebo group at the completion of therapy, and at one year following completion (8). Oxandrolone, utilized as a therapy to improve metabolic efficiency, has not yet been implemented in the treatment of newborn infants or patients with congenital heart defects (CHD).

To investigate the effects of oxandrolone on myocardial energy consumption in the SV infants, we developed a neonatal animal model in which SV physiology was mimicked in a lamb by prenatally shunting the aorta to the pulmonary artery (14). Sheep are the species of choice for development of this model because newborn lambs are of similar size (3–5 kg) to human newborns, pregnant ewes typically carry one to three fetuses per pregnancy and both ewes and fetuses are tolerant of the effects of surgical intervention. After birth, the lambs were treated with oxandrolone for the first month of life. The change in myocardial energy utilization with oxandrolone treatment of the lambs was determined by measuring the first order reaction rate (k_f) of the creatine-kinase (CK) reaction in the heart using magnetization transfer ^{31}P-MR spectroscopy (MT-^{31}P-MRS). We also performed cine MRI on the lamb to study the structure and dynamic function of the myocardium and the loading of the left ventricle by evaluating end diastolic volume (EDV), end systolic volume (ESV), stroke volume (SV) and ejection fraction (EF).

^{31}P spectroscopy allows non-invasive monitoring of phosphorous metabolites, and is being investigated as a tool to scrutinize the bioenergetics of many body organs in conditions of both health and disease (15). Several ^{31}P MRS techniques, such as conventional saturation-transfer MRS (ST MRS) (16), four-angle ST (FAST) (17), three acquisition ST (novel strategy method) (18), triple repetition time ST (TRiST) (19), two repetition time ST (TwiST) (20), time-dependent ST (TDST) (21) and Bloch-Siegert four angle ST (BOAST) (22) have been employed to evaluate myocardial pseudo first order rate constant of creatine-kinase reaction in human and animal hearts.

In the present work we adopted three acquisition ST methodology in one-dimensional MT-^{31}P-CSI pulse sequence to study the myocardial energy metabolism in animal models of congenital cardiac malformations.

Theory

The CK reaction is essential for the buffering and rapid regeneration of adenosine triphosphate (ATP) in heart tissue (21). The heart uses this energy to contract. The CK enzyme catalyzes the reaction, in which the exchange of phosphate between ATP and phosphocreatine (PCr) takes place according to the reaction:

$$PCr^{2-} + ADP^{-} + H^{+} \rightleftarrows Cr + ATP^{2-}. \quad [1]$$

The reaction proceeds in both the forward and reverse directions with k_f and k_r as the pseudo first-order forward and reverse rate constants, respectively. One approach to

the quantification of k_f is to saturate γ-ATP so that the reverse reaction brings no magnetization from γ-ATP to PCr. In MT-^{31}P-MRS, a train of sinc radiofrequency (RF) pulses with a narrow bandwidth (75 Hz) is applied to saturate γ-ATP line. The rate equation of longitudinal magnetization of PCr during these saturation pulses is given by modified Bloch equation:

$$\frac{dM_{PCr}(t)}{dt} = \frac{M^{o}_{PCr}(t) - M_{PCr}(t)}{T_1} - k_f M_{PCr}(t). \quad [2]$$

The detailed solution of Equation 2 can be found elsewhere, in (23-25). The expression of k_f obtained by solving this first order differential equation can be written as:

$$k_f = R'_1 \left(1 - \frac{M^{PCr}_{ss}}{M^{o}_{PCr}}\right), \quad [3]$$

where the apparent relaxation rate, R'_1 measured using γ-ATP saturated is given by the following expression:

$$R'_1 = R_1 + k_f = \frac{1}{TR} \ln \left(1 - \frac{M^{PCr}_{TR}}{M^{PCr}_{ss}}\right), \quad [4]$$

where, M^{PCr}_{TR} is the PCr magnetization obtained with a short TR and continuous saturation pulses at γ-ATP and $R_1 = 1/T_1$ is the intrinsic relaxation rate.

Since γ-ATP is separated from PCr only by 2.5 ppm which is about 125 Hz at 3T, the RF pulse used to selectively saturate γ-ATP also partially saturates PCr peak. The rate equation of longitudinal magnetization of PCr incorporating the RF bleed-over effect in the CK reaction is given by the modified Bloch equation (26):

$$\frac{dM_{PCr}(t)}{dt} = \frac{M^{o}_{PCr}(t) - M_{PCr}(t)}{T_1} - k_f M_{PCr}(t) - \eta M_{PCr}(t). \quad [5]$$

Herein, η is the rate of loss of PCr magnetization due to an RF saturation pulse. The value of η can be estimated by measuring the PCr magnetizations with saturation pulse irradiated at +2.5 ppm and +20 ppm on the opposite side of γ-ATP. The expression of RF bleed-over obtained by solving equation 5 can be written as:

$$\eta = \frac{R''_1 M^{PCr}_{ss}}{M_o}\left(\frac{M_0}{M'_0} - 1\right), \quad [6]$$

where M'_0 and M_o are the thermal equilibrium magnetization with saturation pulse irradiated at +2.5 ppm and +20 ppm, respectively and $R_1'' = R_1 + k_f + \eta$.

MATERIALS AND METHODS

Animal Model

Both timed pregnant ewe (that was preferably carried twins/triplets) and the fetuses were anesthetized at approximately 140 days of gestation (term gestation 145 days). The ewe underwent an abdominal incision, and then a uterine incision to allow exposure of the left forelimb and chest of the fetus. A left lateral thoracotomy was performed on the fetus and a 2 mm length of 8.0 mm diameter Gore-Tex vascular graft (a gift of W. L. Gore & Associates, Inc.) was interposed between the ascending aorta and main pulmonary artery. All incisions were closed, and the ewe was awakened from anesthesia. Antibiotics were given to the ewe, intraoperatively and then on a daily basis thereafter, until two days after delivery. Lambs were allowed to deliver spontaneously, and were cared for by the ewe until approximately one month of age (when MR studies were performed). The lambs rejected by the mother were bottle fed. Unoperated twins of the shunted lambs served as controls. Four groups of total nine lambs (~two lambs per group): control (n = 3), shunted (n = 2), oxandrolone-treated (ox-treated) control (n = 2), and ox-treated shunt (n = 2) were created. The ox-treated animals were given 0.1 mg/kg orally twice daily beginning on Day of Life 2. All animal work was performed under a protocol approved by the local Institutional Animal Care and Use Committee (IACUC) and euthanasia was performed in accordance with American Veterinary Medical Association (AVMA) requirements.

Pulse Sequence

Siemens' product pulse sequence, CSI-free induction decay (FID) was modified to implement one-dimensional MT-^{31}P -CSI pulse sequence by adding outer-volume-suppression (OVS) pulses with user-selectable number of iterations, adiabatic-half-passage (AHP) RF pulse for excitation, a train of narrowband RF pulses to saturate γ-ATP, and 1D CSI with correct localization to the existing

functionalities using the pulse sequence development environment software (IDEA, Siemens Medical Solutions, Erlangen, Germany). The schematic timing diagram of MT-^{31}P-CSI is shown in Figure 1.

The 1D MT-CSI protocol for the lamb's heart is detailed in Table 1. Three hard pulses of 400 μs duration and a flip angle of 110° followed by a spoiling gradient were applied to null the longitudinal magnetizations of all metabolites. A sinc RF pulse with bandwidth 75 Hz and flip angle 300° was used as a MT saturation pulse to saturation the γ-ATP for the duration t_{sat} by repetitive application so that the reverse transfer of magnetization from γ-ATP to PCr could not proceed. Six OVS pulses and gradients were applied to prevent the contamination on the ^{31}P signal of the heart from the ^{31}P signal of the chest muscle. An AHP pulse of bandwidth 4 kHz was used for excitation.

Hardware

Most clinical MR systems have a single RF transmit port for both ^{1}H and ^{31}P frequencies. A high power RF switch is positioned prior to the ^{1}H and ^{31}P TR switches as shown in Figure 2 for the automatic switching of the RF pulses to either the ^{1}H or ^{31}P TR switch for ^{1}H MRI or ^{31}P MRS, respectively.

^{1}H/^{31}P Dual-Tuned RF Coils

Due to a low concentration and relatively small gyromagnetic ratio of ^{31}P in human and animal tissue compared to protons (27, 28), a dedicated ^{31}P coil optimized for the ^{31}P nucleus accompanied by a ^{1}H coil for the scout imaging and shimming of the region of interest is required. We built a quadrature ^{31}P coil with dimensions optimized to the heart of lambs aged four to six weeks, and a relatively large ^{1}H linear coil. The detailed explanation for the construction of the coil is given in the author's previous paper (29). The ^{31}P coil consisted of a butterfly loop decoupled with a rectangular loop for a quadrature mode as shown in Figure 3, by adjusting the overlapping

Table 1. The 1D MT-CSI Protocol for the Lambs' Hearts

	Δf_{MT} (ppm)	TR (s)	N_{MzSat}	t_{preSat} (s)	t_{MT} (s)
M_o^{PCr}	0	20	0	0	0
M_{PCr}^{ss}	-2.7	minimum	0	2.5	3.5
M_{PCr}^{Tsat}	-2.7	minimum	2	0	2

CSI = chemical shift imaging; MT = magnetization transfer; TR = repetition time

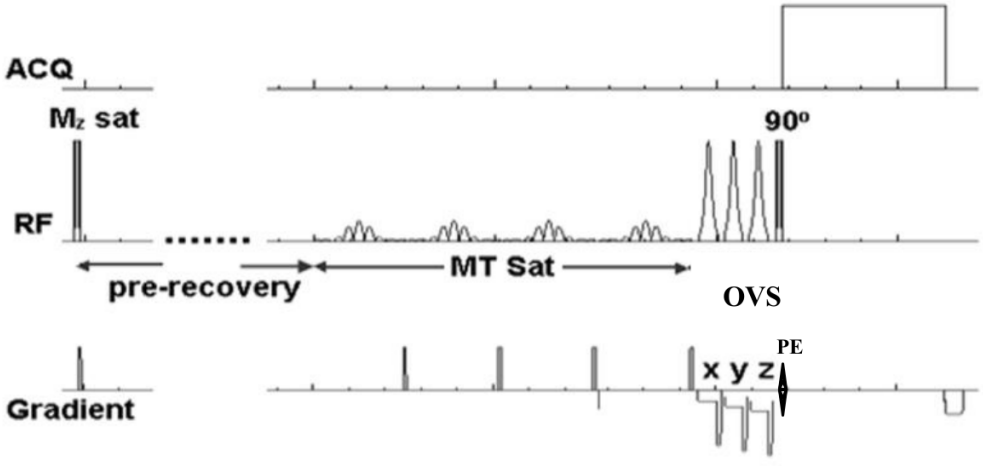

Fig. 1. Timing diagram of pulse sequence, 1D MT-CSI.

region of the coils. The ^{1}H RF coil that surrounded the ^{31}P coil, as shown in the Figure 3, was positioned such that the field produced by the coil would be perpendicular to that produced by the ^{31}P butterfly coil. The coupling between the ^{1}H and ^{31}P rectangular coil was minimized by choosing the large dimension of the ^{1}H coil compared to the rectangular coil. The loaded isolation between the ^{1}H and ^{31}P butterfly coils measured using vector network analyzer (E5061B ENA Series, Agilent Technologies, Englewood, CO, USA) and 250 mL saline bag phantom at the ^{1}H frequency was -23.2 dB and that at the ^{31}P frequency was -28.7 dB while that between the ^{1}H and ^{31}P rectangular coils at the ^{1}H frequency was -22.8 dB and at the ^{31}P frequency was -26.7 dB. Moreover, the ^{31}P coil affects the ^{1}H signal to noise ratio (SNR) far more than the ^{1}H coil affects the ^{31}P SNR (30). This is because ^{31}P coils have relatively high capacitor values compared to the ^{1}H coil, which provides low impedance at the ^{1}H frequency (31). The isolation between the ^{1}H and ^{31}P RF coils at ^{1}H frequency could be further increased by inserting the ^{1}H traps at the ^{31}P coils with a little compromise of the ^{31}P signal. No extra lossy components on the ^{31}P coil were added so that the performance of the ^{31}P coil is same as the same coil on the same frame without ^{1}H coil. The separate coil design for each nucleus allows us to

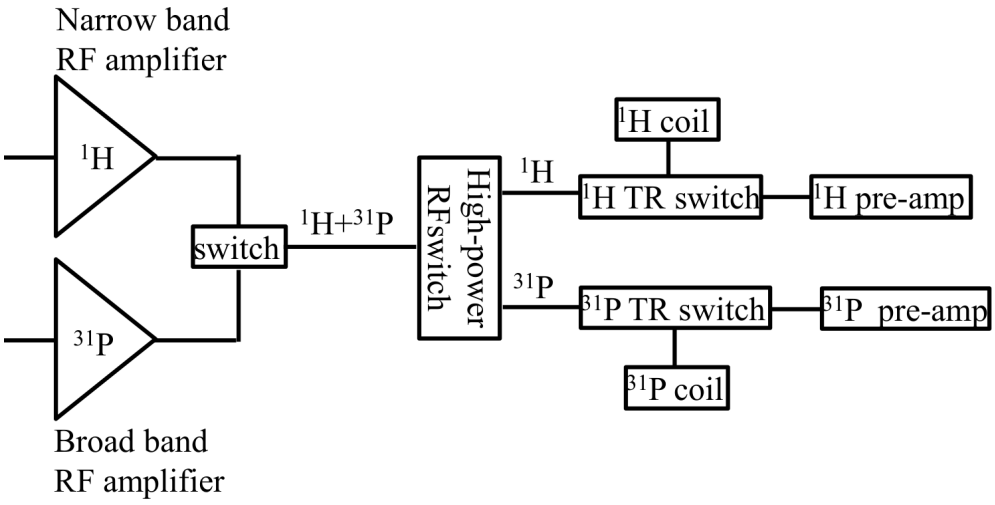

Fig. 2. Block diagram of hardware.

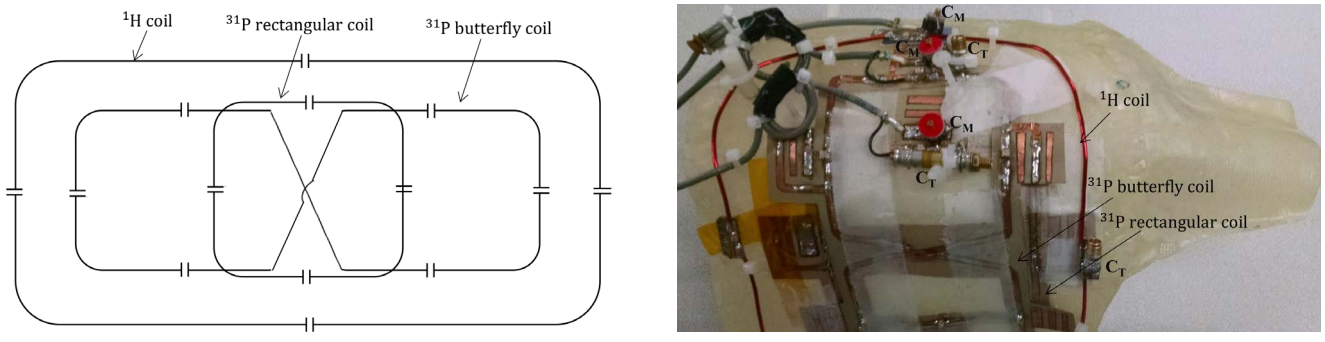

a b

Fig. 3. (a) Circuit diagram and (b) photograph of $^{1}H/^{31}P$ dual tuned RF coils. The ^{31}P loop consisted of a butterfly loop and an inner rectangular loop decoupled geometrically for a quadrature mode. The outer rectangular loop was ^{1}H RF coil whose surface area was made large to minimize the coupling with ^{31}P rectangular loop, and positioned such that it was in quadrature mode with ^{31}P butterfly loop.

independently match and tune the ^{1}H and ^{31}P coils without interference.

T/R and High Power RF Switches

The T/R circuitry for our $^{1}H/^{31}P$ dual-tune RF coil consists of a linear T/R switch for the ^{1}H coil and a quadrature T/R switch for the ^{31}P coil with high-power passive RF switch (29, 32) consisting of two parallel LC trap circuits placed prior to the T/R switches to automatically direct the ^{1}H RF pulse to the ^{1}H T/R switch during ^{1}H MRI and the ^{31}P RF pulse to the ^{31}P T/R switch during ^{31}P MRS.

MRI Experiments

The MT-^{31}P-MRS experiments were carried out on nine lambs aged four to six weeks and in four groups: control (n = 3), ox-treated control (n = 2), shunted (n = 2) and ox-treated shunted (n = 2), using the custom $^{1}H/^{31}P$ double tuned surface transmit/receive coil and $^{1}H/^{31}P$ T/R switch described above on a 3T clinical MRI system (Tim-Trio, Siemens Medical Solutions, Erlangen, Germany). Lambs were anesthetized with 2% isoflurane mixed with oxygen throughout the experiment. The heart rate was monitored using an MR Monitoring System (Medrad Veris model 8600, Medrad Inc. One Medrad Drive Indianola, PA, USA). The RF coils were matched and tuned with the lamb in the scanner using portable RF sweeper probe tuner (405 NV+, Morris Instruments Inc., Ottawa, Ontario, Canada).

^{1}H MR anatomical images were first acquired with the lamb in the scanner (in a feet first left lateral position) to determine the position of RF coils using the localizer. A ^{1}H marker attached to the center of the $^{1}H/^{31}P$ coil was used to adjust coil at the position of heart. The ovine heart was then shimmed to homogenize the B_0 field over the region of heart. Cardiac-triggered, 1D CSI with eight phase encodes and saturation bands on the chest to minimize contamination from the chest muscle were used for ^{31}P spectroscopy. Three experiments were carried out to measure kf. M^{o}_{PCr} was obtained using TR = 20 sec with no MT and M_z saturation pulses, M^{TR}_{PCr} using three hard RF pulses with flip angle 300° as M_z saturation RF and a spoiling gradient pulses followed by MT saturation pulses at -2.7 ppm away from PCr (at the position of γ-ATP) for 2 sec, and M^{ss}_{PCr} was measured with pre-saturation delay of 2.1 sec and MT saturation at -2.7 ppm for 3.5 second (18). The total scan time for measuring M^{o}_{PCr}, M^{ss}_{PCr}, and M^{TR}_{PCr} was 37 minutes 40 seconds. The value of RF bleed over was obtained by measuring M_0 and M'_0 and using equation [6]. The thermal equilibrium magnetization, M'_0 under RF bleed-over was measured by irradiating saturation RF pulses at +2.5 ppm for t_{sat} = 20 s. The same experiment was repeated to measure thermal equilibrium magnetization, M_o without RF bleed-over effect by irradiating saturation RF pulses at +20 ppm (26). All experiments were performed with a receiver bandwidth of 2.5 kHz and 512 data points.

Only four out of the nine lambs (i.e. one in each group of control, shunted, ox-treated control, and ox-treated shunted lambs) underwent cine MRI after ^{31}P MRS using the standard Siemens' coil (Flex Large 4, a 3T Tim) as a receiver and the body coil as a transmitter. Long-axis and short axis scout images were acquired for planning short axis cine images. Cine images covering the whole heart in short axis orientation were acquired using TRUFI (true fast imaging with steady state free precession) pulse sequence with retrospective ECG gating. The imaging parameters were: typical field of view (FOV) = 260 × 142 mm^2, typical matrix size 208 × 114, in-plane resolution = 1.25 × 1.25 mm, contiguous stack of slices of 6 mm thickness, TE/TR = 1.48 ms/3.4 ms, flip angle = 40°, temporal resolution = 23.6 ms.

The raw data for the ^{31}P MRS was processed using home-developed processing software in Python language that performs 10 Hz Gaussian and Lorentzian broadening, zero filling to 4-k of data points, fast Fourier transformation, and interactive zeroth and first order phase correction. The magnetization of PCr and ATP in myocardium was measured as the area under the respective resonance peaks.

The cine data were processed manually using Argus software (Siemens Healthcare) to calculate end diastolic volume (EDV), end systolic volume (ESV), stroke volume (SV) and ejection fraction (EF). The papillary musculature was excluded from the calculation.

RESULTS

Figure 4a shows an example of localizer image with 1D CSI grid (white) and green rectangle as shim region of *in vivo* lamb heart obtained with the custom made $^{1}H/^{31}P$ double tuned RF coils. Figure 4b-e are the representative stacked plots of ^{31}P MR spectra from control (triplet), shunted (triplet), ox-treated shunted (doublet) and the ox-treated control (doublet) lambs, respectively. Blue, green and red spectra indicate M^{o}_{PCr} M^{ss}_{PCr}, and M^{TR}_{PCr}, respectively. The values of k_f, SNR of the M^{o}_{PCr} peak obtained from these spectra, EDV, ESV, SV, and EF are listed in Table 2. The low value of SNR of M^{o}_{PCr} reflects the poor shimming compared to the higher value. The kf of the triplet shunted lamb is

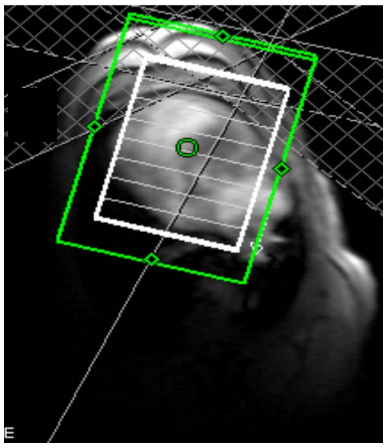

a

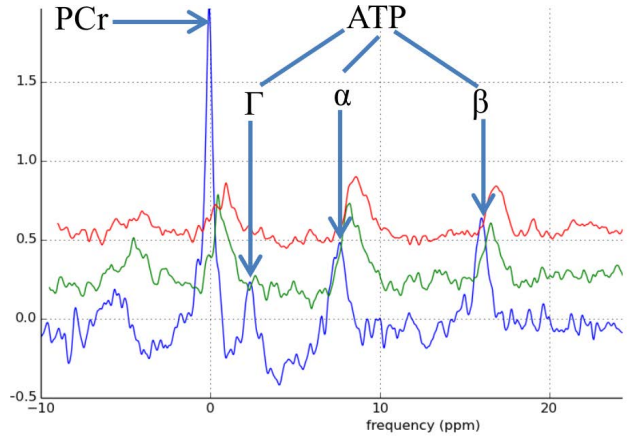

b

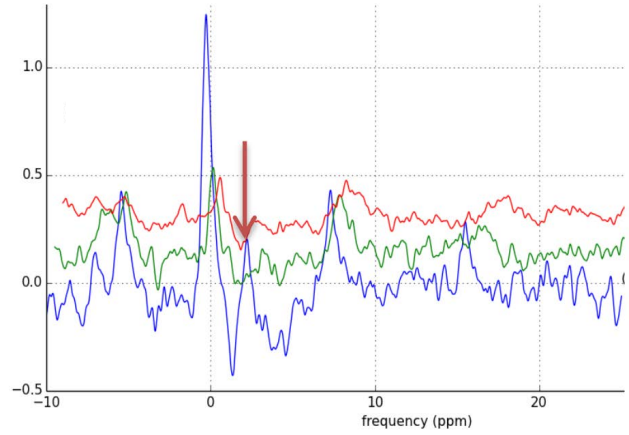

c

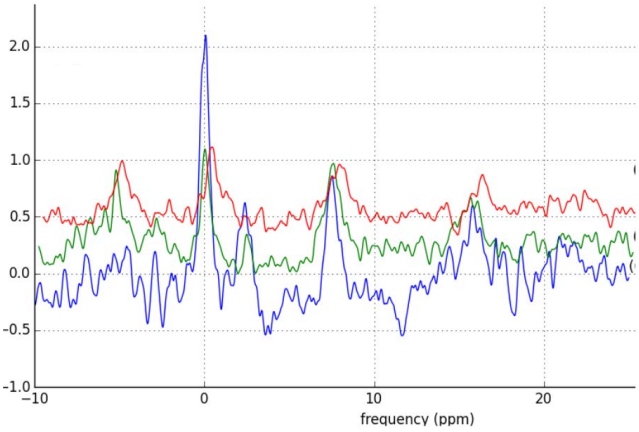

d

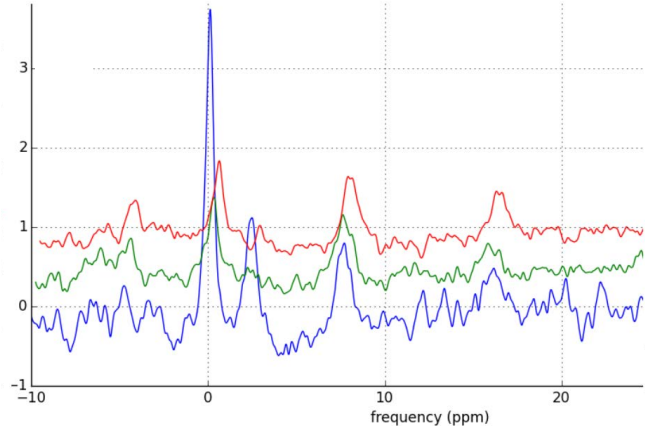

e

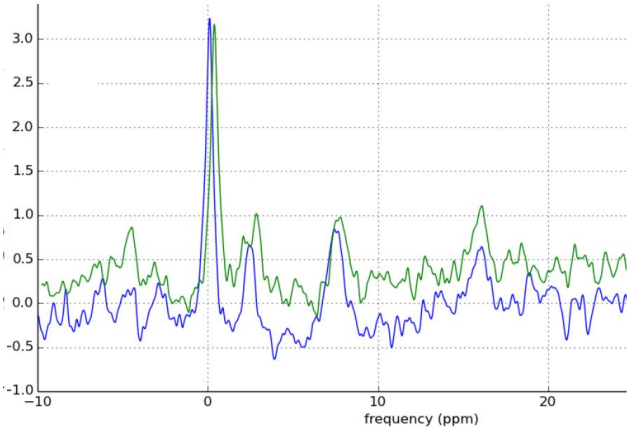

f

Fig. 4. (a) A scout image with 1D CSI grid with green rectangle as a shim region. Saturation bands were used on the chest wall to avoid the contamination on the ^{31}P signal of heart from the chest wall. (b-e) *in-vivo* stacked plots of ^{31}P MR spectra of control (triplet), shunted (twin), and ox-treated control (twin) lamb. Blue, green and red spectra indicate M^{o}_{PCr} (equilibrium), M^{ss}_{PCr} (saturation pulse for 3.5 second and pre-saturation time of 2.5 second), and M^{TR}_{PCr} (saturation pulse for two seconds), respectively. The arrows indicate the positions where saturation pulse is applied. (f) ^{31}P spectra with (green) and without (blue) RF bleed-over effect. There is a decrease in PCr peak due to RF bleed-over effect.

0.09 s^{-1} which is much smaller than either of the control lambs (0.22 s^{-1} or 0.28 s^{-1}) of the same set of triplets. The k_f of the ox-treated shunted lamb of the last doublet is 0.30 s^{-1} which seems to demonstrate the increase of k_f with oxndrolone treatment toward a normal value, or its ox-treated control doublet (k_f = 0.31 s^{-1}). Figure 4f is the spectra for computing the value of RF bleed-over where blue and green spectra are with and without RF bleed-over effect, respectively. The RF bleed-over was found to be 2.8%.

Figure 5 shows an example of the short axis images

Table 2. k_f, Signal to Noise Ratio (SNR) of M_o^{PCr}, End Diastolic Volume (EDV), End Systolic Volume (ESV), Systolic Volume (SV), and Ejection Fraction (EF) of Different Groups of Lambs

Lamb type	Lamb	K_f (s^{-1})	SNR (M_o^{PCr})	EDV (mL)	ESV (mL)	SV (mL)	EF (%)
Triplet (~ 4 weeks)	Control	0.22	49.75	31.0	16.4	14.6	47.2
	Shunted	0.09	25.0				
	Control	0.28	23.75				
Twin (~8 weeks)	Control	0.36	71.0				
	Shunted	0.28	67.0	103.2	69.0	34.2	31.3
Single (~4 weeks)	Ox-treated shunt	0.32	37.7				
Twin (~6 weeks)	Ox-treated control	0.15	34.7				
	Shunted stillborn	-					
Twin (~5 weeks)	Ox-treated control	0.31	56.6	48.6	25.2	23.4	48.1
	Ox-treated shunt	0.30	30.5	100.5	62.5	38.0	37.8

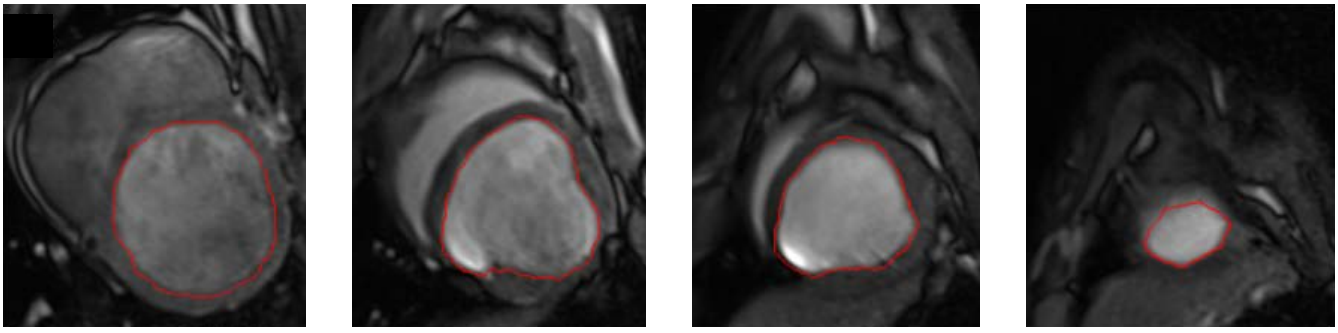

a

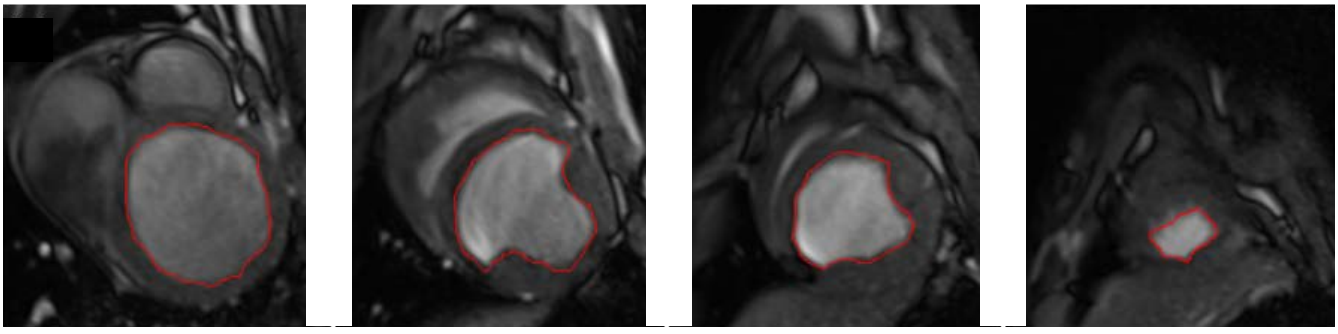

b

Fig. 5. Representative short axis images of shunted lamb with (a) diastolic and (b) systolic contours (red) drawn using Argus software.

of a shunted lamb heart with red contours placed on endocardial myocardial borders from base to apex on all slices pertaining to (a) end diastole and (b) end systole. The papillary muscles are excluded from the contours. Similar contours were drawn for other lambs (not shown) in order to calculate left ventricular parameters. The EF for controlled, shunted, ox-treated control, and ox-treated shunt were 47.2%, 31.3%, 48.1%, and 37.8% respectively. The EDV of the shunted (103.2 mL) or ox-treated shunted lamb (100.5 mL) was two to three times larger than the EDV of either the control (31 mL) or the ox-treated control lamb (48.6 mL), which was expected for volume overloaded hearts.

DISCUSSION AND CONCLUSION

The RF coil and T/R switches were developed to optimize the SNR of the ^{31}P signal and enable ^{1}H/^{31}P dual nuclear MRI/S automatically without the need to physically move and replace either the RF coil or T/R switch during the experiment. We implemented MT saturation technique in 1D CSI pulse sequence to measure k_f in different groups of ovine hearts (as mentioned above) at 3T. An AHP pulse was used to generate a uniform excitation over the region of interest using the quadrature ^{31}P surface coil.

This study is the first to measure k_f and cardiac volume in surgically created SV and ox-treated lambs. We studied oxandrolone's effect on myocardial energetics and function not because it's a new drug, but because we are proposing a novel and therapeutic use for the substance for the purpose of treating growth failure in SV infants. The k_f of the *in vivo* ovine heart was measured using novel strategy method (three acquisition method) (18) with drastically shorter total data acquisition time compared to the conventional approach which requires progressive saturation experiments with long pre and MT saturation times to evaluate M_{PCr}^{ss} and $R_0^{'}$. The PCr peak in blue spectra in Figure 4b-e, for measuring M_{PCr}^{o}, was reduced in green spectra for measuring M_{PCr}^{ss} due to the application of MT pulses at the position of γ-ATP peak (to suppress reverse magnetization from γ-ATP to PCr) for 3.5 seconds, and even further reduced in red spectra for measuring M_{PCr}^{TR} due to short TR and MT saturation pulses (applied for two seconds), as used in this acquisition.

It is fairly reasonable to compare the k_f values between the lambs of same biologic twin or triplet. The values of k_f obtained from our results show that, compared with the control heart of the same twins/triplets, the forward reaction rate constant of CK reaction is significantly lower in a shunted heart, and it is increased in the ox-treated heart compared to the shunted heart which may indicate the increase in the rate of energy production in the ox-treated lamb. This result is consistent with the previous studies on *in vivo* human hearts, which reported substantial decreases in k_f in failing hypertrophic myocardium compared to healthy myocardium (33-35) and on seven month old isolated cardiomyopathic hamster heart which showed an increase in the CK flux with enalapril-treatment (36). The value of k_f for the shunted or control heart of the triplets is smaller than that in the twins. The value of k_f for the control and ox-treated control lamb of the last twins of Table 2 is approximately same as expected. The k_f values of shunted and control lambs of one twin or triplet is different from another twin or triplet lambs. This may be due to several reasons. The triplet shunt may not get enough nutrients than the twin shunt before and after its birth. Those lambs which are rejected by the ewe after birth were bottle-fed. One lamb may be much sicker than the other. The triplet shunt was scanned when it was ~ one month old and the twin shunt was scanned when it was ~ two months old. Chesky et al. (37) from the ^{31}P MRS on the male Fischer rat have shown that the myocardial creatine phosphokinase activity rises from one month of age to a maximum two months of age. There may not be the same experimental situation for the lambs though we tried hard to equalize the circumstance as much as possible. It might be that they were simply scanned on different dates.

Several methods, such as cardiovascular ultrasound (38), angiocardiography (39), and computed tomography (40) have been used to quantitatively evaluate the ESV, EDV, SV, and EF of the left ventricle. These methods have certain constraints and drawbacks. For instance, computed tomography is carcinogenic to the patient, cardiovascular ultrasound method requires geometric premise, etc. As an alternative to these methods, cardiac MRI is a non-invasive method that has been frequently used as a standard tool for the cardiac volume measurements (41, 42). In the present study, we used cine MRI for the volume measurements of *in vivo* ovine heart. The cine MRI measurement of the ovine heart shows that EF of control lamb is greater than that of the shunted heart and is similar to that of the ox-treated control lamb. There is some improvement of EF with oxandrolone treatment, as expected. The EDV and ESV of ox-treated shunts are greater than those of the ox-treated controls, which indicates the greater remodeling in

the ventricle of the shunted lamb. Further studies on more lambs, with and without, surgically created SV physiology are needed for proper statistical analyses to confirm these findings.

Acknowledgments

This work was partly supported by NSF CBET 1133908 grant, Margolis Foundation, NMSS Research Grant RG 5233-A-2 and Primary Children's Hospital Foundation Integrated Science Award of University of Utah.

REFERENCES

1. Hancock Friesen CL, Forbess JM. Surgical management of the single ventricle. Prog Pediatr Cardiol 2002;16:47-68
2. Schwalbe-Terilli CR, Hartman DH, Nagle ML, et al. Enteral feeding and caloric intake in neonates after cardiac surgery. Am J Crit Care 2009;18:52-57
3. Anderson JB, Beekman RH 3rd, Eghtesady P, et al. Predictors of poor weight gain in infants with a single ventricle. J Pediatr 2010;157:407-413, 413 e401
4. Nydegger A, Bines JE. Energy metabolism in infants with congenital heart disease. Nutrition 2006;22:697-704
5. Leitch CA. Growth, nutrition and energy expenditure in pediatric heart failure. Prog Pediatr Cardiol 2000;11:195-202
6. Di Maria MV, Glatz AC, Ravishankar C, et al. Supplemental tube feeding does not mitigate weight loss in infants with shunt-dependent single-ventricle physiology. Pediatr Cardiol 2013;34:1350-1356
7. Fox-Wheeler S, Heller L, Salata CM, et al. Evaluation of the effects of oxandrolone on malnourished HIV-positive pediatric patients. Pediatrics 1999;104:e73
8. Porro LJ, Herndon DN, Rodriguez NA, et al. Five-year outcomes after oxandrolone administration in severely burned children: a randomized clinical trial of safety and efficacy. J Am Coll Surg 2012;214:489-502; discussion 502-484
9. Rosenfeld RG, Frane J, Attie KM, et al. Six-year results of a randomized, prospective trial of human growth hormone and oxandrolone in Turner syndrome. J Pediatr 1992;121:49-55
10. Wilson DM, McCauley E, Brown DR, Dudley R. Oxandrolone therapy in constitutionally delayed growth and puberty. Bio-Technology General Corporation Cooperative Study Group. Pediatrics 1995;96:1095-1100
11. Hart DW, Wolf SE, Ramzy PI, et al. Anabolic effects of oxandrolone after severe burn. Ann Surg 2001;233:556-564
12. Przkora R, Jeschke MG, Barrow RE, et al. Metabolic and hormonal changes of severely burned children receiving long-term oxandrolone treatment. Ann Surg 2005;242:384-389, discussion 390-381
13. Wolf SE, Thomas SJ, Dasu MR, et al. Improved net protein balance, lean mass, and gene expression changes with oxandrolone treatment in the severely burned. Ann Surg 2003;237:801-810; discussion 810-801
14. Reddy VM, Meyrick B, Wong J, et al. In utero placement of aortopulmonary shunts. A model of postnatal pulmonary hypertension with increased pulmonary blood flow in lambs. Circulation 1995;92:606-613
15. Neubauer S. The failing heart--an engine out of fuel. N Engl J Med 2007;356:1140-1151
16. Bottomley PA, Hardy CJ. Mapping creatine kinase reaction rates in human brain and heart with 4 tesla saturation transfer 31P NMR. J Magn Reson 1992;99:443-448
17. Bottomley PA, Ouwerkerk R, Lee RF, Weiss RG. Four-angle saturation transfer (FAST) method for measuring creatine kinase reaction rates in vivo. Magn Reson Med 2002;47:850-863
18. Xiong Q, Li Q, Mansoor A, et al. Novel strategy for measuring creatine kinase reaction rate in the in vivo heart. Am J Physiol Heart Circ Physiol 2009;297:H1010-1019
19. Schar M, El-Sharkawy AM, Weiss RG, Bottomley PA. Triple repetition time saturation transfer (TRiST) 31P spectroscopy for measuring human creatine kinase reaction kinetics. Magn Reson Med 2010;63:1493-1501
20. Schar M, Gabr RE, El-Sharkawy AM, Steinberg A, Bottomley PA, Weiss RG. Two repetition time saturation transfer (TwiST) with spill-over correction to measure creatine kinase reaction rates in human hearts. J Cardiovasc Magn Reson 2015;17:70
21. Bashir A, Gropler R. Reproducibility of creatine kinase reaction kinetics in human heart: a (31) P time-dependent saturation transfer spectroscopy study. NMR Biomed 2014;27:663-671
22. Clarke WT, Robson MD, Neubauer S, Rodgers CT. Creatine kinase rate constant in the human heart measured with 3D-localization at 7 tesla. Magn Reson Med 2017;78:20-32
23. Ugurbil K. Magnetization-transfer measurements of individual rate constants in the presence of multiple reactions. J Magn Reson 1985;64:207-219
24. Kingsley-Hickman PB, Sako EY, Mohanakrishnan P, et al. 31P NMR studies of ATP synthesis and hydrolysis kinetics in the intact myocardium. Biochemistry 1987;26:7501-7510
25. Kingsley PB, Monahan WG. Corrections for off-resonance effects and incomplete saturation in conventional (two-site) saturation-transfer kinetic measurements. Magn

Reson Med 2000;43:810-819
26. Jeong EK, Sung YH, Kim SE, et al. Measurement of creatine kinase reaction rate in human brain using magnetization transfer image-selected in vivo spectroscopy (MT-ISIS) and a volume 31P/1H radiofrequency coil in a clinical 3-T MRI system. NMR Biomed 2011;24:765-770
27. Potter W, Wang L, McCully K, Zhao Q. Evaluation of a new 1H/31P dual-tuned birdcage coil for 31P spectroscopy. Concepts Magn Reson Part B Magn Reson Eng 2013;43:90-99
28. Thapa B, Dahl M, Frank D, Burch P, Jeong EK. Quantitaive evaluation of the first order rate constant of creatine-kinase reaction in ovine heart using magntization transfer 31P magnetic resonance spectroscopy (MT-^{31}P-MRS). In Proceedings of the 23rd Scientific Meeting of International Society for Magnetic Resonance in Medicine. Toronto, 2015:2003
29. Thapa B, Kaggie J, Sapkota N, Frank D, Jeong EK. Design and development of a general-purpose transmit/receive (T/R) switch for MRI, compatible for a linear, quadrature and double-tuned RF coil. Concepts Magn Reson Part B Magn Reson Eng 2016;46B:56-65
30. Adriany G, Gruetter R. A half-volume coil for efficient proton decoupling in humans at 4 tesla. J Magn Reson 1997;125:178-184
31. Kaggie JD, Hadley JR, Badal J, et al. A 3 T sodium and proton composite array breast coil. Magn Reson Med 2014;71:2231-2242
32. Thapa B, Kaggie J, Sapkota N, Jeong EK. Design and develpoment of general purpose transmit-receive (TR) switch for a linear, quadrature and dual tuned coils. In Proceedings of the 23rd Scientific Meeting of International Society for Magnetic Resonance in Medicine. Toronto, 2015:1784
33. Weiss RG, Gerstenblith G, Bottomley PA. ATP flux through creatine kinase in the normal, stressed, and failing human heart. Proc Natl Acad Sci U S A 2005;102:808-813
34. Smith CS, Bottomley PA, Schulman SP, Gerstenblith G, Weiss RG. Altered creatine kinase adenosine triphosphate kinetics in failing hypertrophied human myocardium. Circulation 2006;114:1151-1158
35. Abraham MR, Bottomley PA, Dimaano VL, et al. Creatine kinase adenosine triphosphate and phosphocreatine energy supply in a single kindred of patients with hypertrophic cardiomyopathy. Am J Cardiol 2013;112:861-866
36. Nascimben L, Friedrich J, Liao R, Pauletto P, Pessina AC, Ingwall JS. Enalapril treatment increases cardiac performance and energy reserve via the creatine kinase reaction in myocardium of Syrian myopathic hamsters with advanced heart failure. Circulation 1995;91:1824-1833
37. Chesky JA, Rockstein M, Lopez T. Changes with age of myocardial creatine phosphokinase in the male Fischer rat. Mech Ageing Dev 1980;12:237-243
38. Chen C, Guerrero JL, Vazquez de Prada JA, et al. Intracardiac ultrasound measurement of volumes and ejection fraction in normal, infarcted, and aneurysmal left ventricles using a 10-MHz ultrasound catheter. Circulation 1994;90:1481-1491
39. Wisneski JA, Pfeil CN, Wyse DG, Mitchell R, Rahimtoola SH, Gertz EW. Left ventricular ejection fraction calculated from volumes and areas: underestimation by area method. Circulation 1981;63:149-151
40. Rich S, Chomka EV, Stagl R, Shanes JG, Kondos GT, Brundage BH. Determination of left ventricular ejection fraction using ultrafast computed tomography. Am Heart J 1986;112:392-396
41. Bellenger NG, Burgess MI, Ray SG, et al. Comparison of left ventricular ejection fraction and volumes in heart failure by echocardiography, radionuclide ventriculography and cardiovascular magnetic resonance; are they interchangeable? Eur Heart J 2000;21:1387-1396
42. Malayeri AA, Johnson WC, Macedo R, Bathon J, Lima JA, Bluemke DA. Cardiac cine MRI: quantification of the relationship between fast gradient echo and steady-state free precession for determination of myocardial mass and volumes. J Magn Reson Imaging 2008;28:60-66